Available online at www.sciencedirect.com
SCIENCE DIRECT®
C. R. Mecanique 333 (2005) 884–895
COMPTES RENDUS
MECANIQUE
http://france.elsevier.com/direct/CRAS2B/

Fluid–solid interactions: modeling, simulation, bio-mechanical applications

Direct simulation of the motion of neutrally buoyant balls in a three-dimensional Poiseuille flow

Tsorng-Whay Pan *, Roland Glowinski

University of Houston, Department of Mathematics, Houston, TX 77204, USA

Available online 17 November 2005

Abstract

In a previous article the authors introduced a Lagrange multiplier based fictitious domain method. Their goal in the present article is to apply a generalization of the above method to: (i) the numerical simulation of the motion of neutrally buoyant particles in a three-dimensional Poiseuille flow; (ii) study – via direct numerical simulations – the migration of neutrally buoyant balls in the tube Poiseuille flow of an incompressible Newtonian viscous fluid. Simulations made with one and several particles show that, as expected, the Segré–Silberberg effect takes place. ***To cite this article: T.-W. Pan, R. Glowinski, C. R. Mecanique 333 (2005).***

Résumé

Simulation directe du mouvement de particules sphériques de flottabilité neutre dans un écoulement de Poiseuille tri-dimensionnel. Dans un autre article, les auteurs ont introduit une méthode de domaine fictif avec multiplicateurs de Lagrange. Leur objectif dans le présent article est d'appliquer une généralisation de la méthode ci-dessus à : (i) la simulation numérique du mouvement de particules interagissant avec un écoulement de Poiseuille tri-dimensionnel lorsque fluide et particules ont la même densité ; (ii) l'étude – par simulation numérique directe – de la migration de particules sphériques interagissant avec l'écoulement de Poisseuille, dans un tube de section ciculaire, d'un fluide Newtonien, visqueux, incompressible, de même densité que les particules. Comme prévu, ces simulations, effectuées avec une ou plusieurs particules, mettent en evidence l'effet de Segré–Silberberg. ***Pour citer cet article : T.-W. Pan, R. Glowinski, C. R. Mecanique 333 (2005).***

Keywords: Computational fluid mechanics; Particulate flow; Solid–liquid flow; Neutrally buoyant particles; Fictitious domain methods; Distributed Lagrange multipliers; Operator-splitting methods; Finite element methods; Segré–Silberberg effect

Mots-clés : Mécanique des fluides numérique ; Ecoulements particulaires ; Ecoulements solide–liquide ; Particules de flottabilité neutre ; Méthodes de domaines fictifs ; Multiplicateurs de Lagrange distribués ; Méthodes de décomposition d'opérateurs ; Méthodes d'éléments finis ; Effet de Segré–Silberberg

1. Introduction

The problem of particle motions in shear flows is crucially important in many engineering areas, such as the handling of fluid–solid mixtures in slurries, colloids, and fluidized beds. The experiments of Segré and Silberberg [1,2]

* Corresponding author.
E-mail address: pan@math.uh.edu (T.-W. Pan).

1631-0721/$ – see front matter
doi:10.1016/j.crme.2005.10.006

have had a large influence on fluid mechanics studies of migration and lift of particles. They studied the migration of dilute suspensions of neutrally buoyant spheres in a pipe flow at Reynolds numbers between 2 and 700. The particles migrate away from the wall and centerline and accumulate at about 0.6 of the pipe radius from the centerline. Karnis el al. [3] verified the same phenomenon and observed that particles migrate faster for larger flow rate, closer to the wall for larger flow rate and closer to the axis for larger rigid spheres. The 'anomalous' motion observed is attributed to the nonlinear effect of inertia. Comprehensive reviews of experimental and theoretical works have been given by Brenner [4], Cox and Mason [5], Leal [6], Feuillebois [7], and McLaughlin [8] among others.

Direct numerical simulations have been used for understanding particle motion in shear flows. Feng el al. [9] investigated the motion of neutrally buoyant and non-neutrally buoyant circular particles in plane Couette and Poiseuille flows using a finite element method and obtained qualitative agreement with the results of perturbation theories and of experiments. Inamuro et al. [10] used the lattice Boltzmann method to study the motions of neutrally buoyant circular disks in a pressure driven plane Poiseuille flow. The Segré–Silberberg effect was found. They found that the equilibrium position of the particle is closer to the wall as the Reynolds number increases from about 12 to 96; but moves away from the wall as either the diameter of disk or the length of the channel is increased. Pan and Glowinski have generalized the *distributed Lagrange multiplier/fictitious domain method* (DLM/FD) for the numerical simulation of particulate flow (see [11–13]) to the case where the particles are neutrally buoyant in [14] for two-dimensional flows and confirmed via simulations that the phenomenon of collisions between particles is one of the key factors driving particles to the central region of the plane Poiseuille flow. Concerning three-dimensional computational results, Yang et al. [15] have recently studied the migration of a neutrally buoyant ball in a tube Poiseuille flow by using an arbitrary Lagrangian–Eulerian moving mesh technique.

In this article, we have extended the methodology in [14] to three-dimensional flows and performed simulations of the migration of neutrally buoyant balls in a tube Poiseuille flow. The content of this article is as follows: in Section 2, we discuss a fictitious domain formulation of the model problem concerning the case of the neutrally buoyant balls moving freely in a three-dimensional Poiseuille flow; then in Section 3 we discuss briefly the time and space discretization issues, and in Section 4 we present and comment the results of numerical experiments involving one and five neutrally buoyant balls.

2. A fictitious domain formulation of the model problem

All the fluid–solid interactions to be considered in this article concern the flow of fluid–solid particle mixtures in a cylindrical tube (denoted by $\mathbf{T}$ in the sequel) with a circular cross-section. In order to take a full advantage of the fictitious domain approach we will embed $\mathbf{T}$ in a cylindrical tube (denoted by Ω) with a square cross section whose edge length is equal to the diameter of the $\mathbf{T}$ cross-section. We will start our discussion with a one particle situation. Therefore, let $\Omega \subset \mathbb{R}^3$ be a rectangular parallelepiped. We suppose that Ω is filled with a *Newtonian incompressible viscous fluid* (of *density* ρ_f and *viscosity* μ_f) and that it contains a moving neutrally buoyant rigid particle B centered at $\mathbf{G} = \{G_1, G_2, G_3\}^t$ of *density* ρ_f, as shown in Fig. 1, which shows also the inclusion in Ω of the cylinder $\mathbf{T}$ mentioned above; we suppose that the central axis of both cylinders is parallel to the x_3-axis. The flow is modeled by the *Navier–Stokes equations* while the particle motion is described by the *Euler–Newton's equations*. We introduce (with $\mathrm{d}\mathbf{x} = \mathrm{d}x_1\,\mathrm{d}x_2\,\mathrm{d}x_3$) the following functional spaces:

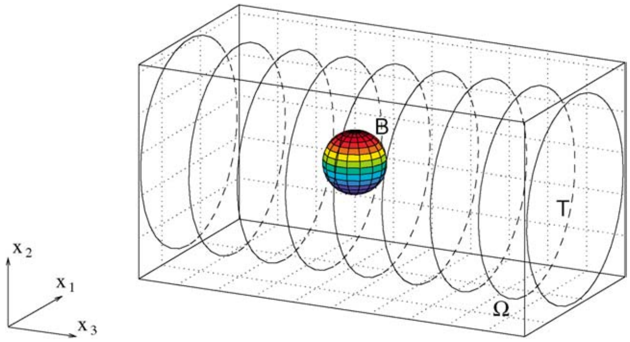

Fig. 1. An example of three-dimensional flow region with one rigid body.

$$W_{0,P} = \{\mathbf{v} \mid \mathbf{v} \in (H^1(\Omega))^3,\ \mathbf{v} = \mathbf{0} \text{ on the top, bottom, front, and back of } \Omega \text{ and}$$
$$\mathbf{v} \text{ is periodic in the } x_3 \text{ direction}\}$$
$$L_0^2 = \left\{q \mid q \in L^2(\Omega), \int_\Omega q \,\mathrm{d}\mathbf{x} = 0\right\}$$
$$\Lambda_0(t) = \{\boldsymbol{\mu} \mid \boldsymbol{\mu} \in (H^1(B(t)))^3,\ \langle \boldsymbol{\mu}, \mathbf{e}_i\rangle_{B(t)} = 0,\ \langle \boldsymbol{\mu}, \mathbf{e}_i \times \overrightarrow{\mathbf{Gx}}\rangle_{B(t)} = 0,\ i = 1, 2, 3\}$$
$$\Lambda_T = \{\boldsymbol{\mu} \mid \boldsymbol{\mu} \in (H^1(\Omega \setminus \overline{\mathbf{T}}))^3,\ \boldsymbol{\mu} \text{ is periodic in the } x_3 \text{ direction}\}$$

where $\mathbf{e}_1 = \{1, 0, 0\}^t$, $\mathbf{e}_2 = \{0, 1, 0\}^t$, $\mathbf{e}_3 = \{0, 0, 1\}^t$, and where $\langle \cdot, \cdot\rangle_{B(t)}$ (resp., $\langle \cdot, \cdot\rangle_T$) is an inner product on $\Lambda_0(t)$ (resp., Λ_T) (see [13] (Section 5) and [11] (Chapter 8) for further information on the choice of $\langle \cdot, \cdot\rangle_{B(t)}$). Above, and from now on, periodicity in the x_3 direction means periodicity of period L, L being the common length of the truncated cylinders Ω and $\mathbf{T}$. Then, the distributed Lagrange multiplier based fictitious domain formulation for the flow around a freely moving neutrally buoyant particle inside a cylindrical tube reads as follows (see [11–13] for a detailed discussion of the non-neutrally buoyant case):

For a.e. $t > 0$, find $\mathbf{u}(t) \in W_{0,P}$, $p(t) \in L_0^2$, $\mathbf{V_G}(t) \in \mathbb{R}^3$, $\mathbf{G}(t) \in \mathbb{R}^3$

$\boldsymbol{\omega}(t) \in \mathbb{R}^3$, $\boldsymbol{\lambda}(t) \in \Lambda_0(t)$, $\boldsymbol{\lambda}_T \in \Lambda_T$ such that

$$\begin{cases} \rho_f \displaystyle\int_\Omega \left[\frac{\partial \mathbf{u}}{\partial t} + (\mathbf{u} \cdot \nabla)\mathbf{u}\right] \cdot \mathbf{v} \,\mathrm{d}\mathbf{x} + 2\mu_f \int_\Omega \mathbf{D}(\mathbf{u}) : \mathbf{D}(\mathbf{v}) \,\mathrm{d}\mathbf{x} - \int_\Omega p \nabla \cdot \mathbf{v} \,\mathrm{d}\mathbf{x} - \langle \boldsymbol{\lambda}, \mathbf{v}\rangle_{B(t)} - \langle \boldsymbol{\lambda}_T, \mathbf{v}\rangle_T \\ \quad = \rho_f \displaystyle\int_\Omega \mathbf{g} \cdot \mathbf{v} \,\mathrm{d}\mathbf{x} + \int_\Omega \mathbf{F} \cdot \mathbf{v} \,\mathrm{d}\mathbf{x}, \quad \forall \mathbf{v} \in W_{0,P} \end{cases} \tag{1}$$

$$\int_\Omega q \nabla \cdot \mathbf{u}(t) \,\mathrm{d}\mathbf{x} = 0, \quad \forall q \in L^2(\Omega) \tag{2}$$

$$\langle \boldsymbol{\mu}, \mathbf{u}(t)\rangle_{B(t)} = 0, \quad \forall \boldsymbol{\mu} \in \Lambda_0(t) \tag{3}$$

$$\langle \boldsymbol{\mu}_T, \mathbf{u}(t)\rangle_T = 0, \quad \forall \boldsymbol{\mu}_T \in \Lambda_T \tag{4}$$

$$\frac{\mathrm{d}\mathbf{G}}{\mathrm{d}t} = \mathbf{V_G} \tag{5}$$

$$\mathbf{V_G}(0) = \mathbf{V_G^0}, \quad \boldsymbol{\omega}(0) = \boldsymbol{\omega}^0, \quad \mathbf{G}(0) = \mathbf{G}^0 = \{G_1^0, G_2^0, G_3^0\}^t \tag{6}$$

$$\mathbf{u}(\mathbf{x}, 0) = \bar{\mathbf{u}}_0(\mathbf{x}) = \begin{cases} \mathbf{u}_0(\mathbf{x}), & \forall \mathbf{x} \in \Omega \setminus \overline{B(0)} \\ \mathbf{V_G^0} + \boldsymbol{\omega}^0 \times \overrightarrow{\mathbf{G}^0\mathbf{x}}, & \forall \mathbf{x} \in \overline{B(0)} \end{cases} \tag{7}$$

In (1)–(7) $\mathbf{u}$ and p denote *velocity* and *pressure*, respectively, $\boldsymbol{\lambda}$ is a *Lagrange multiplier* associated with relation (3) (from (3) the fluid has a rigid body motion in the region occupied by $B(t)$), $\boldsymbol{\lambda}_T$ is a *Lagrange multiplier* associated with relation (4) (from (4), the fluid velocity is $\mathbf{0}$ in $\overline{\Omega} \setminus \mathbf{T}$), $\mathbf{D}(\mathbf{v}) = \frac{1}{2}(\nabla \mathbf{v} + (\nabla \mathbf{v})^t)$, $\mathbf{g}$ denotes *gravity*, $\mathbf{F}$ is an imposed *pressure gradient* pointing in the x_3-direction inside the cylinder $\mathbf{T}$, $\mathbf{V_G}$ is the *translation velocity* of the particle B, and $\boldsymbol{\omega}$ is the *angular velocity* of B. We suppose that the *no-slip* condition holds on ∂B. We also use, if necessary, the notation $\phi(t)$ for the function $\mathbf{x} \to \phi(\mathbf{x}, t)$.

Remark 1. The hydrodynamical forces and torque imposed on the rigid body by the fluid are built in (1)–(7) implicitly (see [12,13] for details), thus we do not need to compute them explicitly in the simulation. Since in (1)–(7) the flow field is defined on the entire domain Ω, it can be computed with a simple structured grid.

Remark 2. In (3), the rigid body motion in the region occupied by the particle is enforced via Lagrange multipliers $\boldsymbol{\lambda}$. To recover the translation velocity $\mathbf{V_G}(t)$ and the angular velocity $\boldsymbol{\omega}(t)$ from $\mathbf{u}(t)$ satisfying (3), we solve the following equations

$$\begin{cases} \langle \mathbf{e}_i, \mathbf{u}(t) - \mathbf{V_G}(t) - \boldsymbol{\omega}(t) \times \overrightarrow{\mathbf{Gx}}\rangle_{B(t)} = 0, & \text{for } i = 1, 2, 3 \\ \langle \mathbf{e}_i \times \overrightarrow{\mathbf{Gx}}, \mathbf{u}(t) - \mathbf{V_G}(t) - \boldsymbol{\omega}(t) \times \overrightarrow{\mathbf{Gx}}\rangle_{B(t)} = 0, & \text{for } i = 1, 2, 3 \end{cases} \tag{8}$$

Remark 3. In (1)–(7), the ball is moving freely inside the cylinder $\mathbf{T}$. If we want to restrict the ball to move along a line parallel and under the central axis of the cylinder and to rotate freely only with respect to the x_1-axis, we have to modify the multiplier space $\Lambda_0(t)$ accordingly. Since we have $\mathbf{V_G} = \{V_{x_1}, V_{x_2}, V_{x_3}\}^t = \{0, 0, V_{x_3}\}^t$ and $\boldsymbol{\omega} = \{\omega_{x_1}, \omega_{x_2}, \omega_{x_3}\}^t = \{\omega_{x_1}, 0, 0\}^t$, the multiplier space $\Lambda_0(t)$ becomes

$$\Lambda_0(t) = \left\{\boldsymbol{\mu} \mid \boldsymbol{\mu} \in \left(H^1\left(B(t)\right)\right)^3,\ \langle \boldsymbol{\mu}, \mathbf{e}_3 \rangle_{B(t)} = 0,\ \langle \boldsymbol{\mu}, \mathbf{e}_1 \times \overrightarrow{\mathbf{Gx}} \rangle_{B(t)} = 0\right\}$$

Via (3) we obtain $V_{x_1} = 0$, $V_{x_2} = 0$, $\omega_{x_2} = 0$ and $\omega_{x_3} = 0$. Let $\mathbf{V}^c_{\mathbf{G}} = \{0, 0, V_{x_3}\}^t$ and $\boldsymbol{\omega}^c = \{\omega_{x_1}, 0, 0\}^t$. To recover V_{x_3} and ω_{x_1} from $\mathbf{u}(t)$ satisfying (3), we solve the following equations

$$\begin{cases} \left\langle \mathbf{e}_3, \mathbf{u}(t) - \mathbf{V}^c_{\mathbf{G}}(t) - \boldsymbol{\omega}^c(t) \times \overrightarrow{\mathbf{Gx}} \right\rangle_{B(t)} = 0 \\ \left\langle \mathbf{e}_1 \times \overrightarrow{\mathbf{Gx}}, \mathbf{u}(t) - \mathbf{V}^c_{\mathbf{G}}(t) - \boldsymbol{\omega}^c(t) \times \overrightarrow{\mathbf{Gx}} \right\rangle_{B(t)} = 0 \end{cases}$$

Remark 4. In (1), $2\int_\Omega \mathbf{D}(\mathbf{u}) : \mathbf{D}(\mathbf{v})\,\mathrm{d}\mathbf{x}$ can be replaced by $\int_\Omega \nabla\mathbf{u} : \nabla\mathbf{v}\,\mathrm{d}\mathbf{x}$ since $\mathbf{u}$ is divergence free and in $W_{0,P}$. This change can make the computation simpler and faster. Also the gravity $\mathbf{g}$ in (1) can be absorbed into the pressure term.

3. Space approximation and time discretization

Concerning the finite element based *space approximation* of $\{\mathbf{u}, p\}$ in problem (1)–(7), we will use the *Bercovier–Pironneau P_1-iso-P_2* finite element approximation (as in Bristeau et al. [16]; see also [11] (Chapter 5)). More precisely, with h a *space discretization step* we introduce a uniform 'tetrahedrization' $\mathcal{T}_h$ of $\overline{\Omega}$ and a twice coarser 'tetrahedrization' $\mathcal{T}_{2h}$. We approximate then $W_{0,P}$, $L^2(\Omega)$ and L^2_0 by the following finite dimensional spaces

$$W_{0,h} = \left\{\mathbf{v}_h \mid \mathbf{v}_h \in \left(C^0(\overline{\Omega})\right)^3,\ \mathbf{v}_h|_T \in (P_1)^3,\ \forall T \in \mathcal{T}_h,\ \mathbf{v}_h = \mathbf{0} \text{ on the top, bottom, front, and back of } \Omega \text{ and } \mathbf{v} \text{ is periodic at } \Gamma \text{ in the } x_3 \text{ direction}\right\} \tag{9}$$

$$L^2_h = \left\{q_h \mid q_h \in C^0(\overline{\Omega}),\ q_h|_T \in P_1,\ \forall T \in \mathcal{T}_{2h}\right\} \tag{10}$$

$$L^2_{0,h} = \left\{q_h \mid q_h \in L^2_h,\ \int_\Omega q_h\,\mathrm{d}\mathbf{x} = 0,\ q_h \text{ is periodic at } \Gamma \text{ in the } x_3 \text{ direction}\right\} \tag{11}$$

respectively; in (9)–(11), P_1 is the space of the polynomials in three variables of degree $\leqslant 1$. A finite dimensional space approximating $\Lambda_0(t)$ is as follows: let $\{\boldsymbol{\xi}_i\}_{i=1}^N$ be a set of points from $\overline{B(t)}$ which cover $\overline{B(t)}$ (uniformly, for example); we define then

$$\Lambda_h(t) = \left\{\boldsymbol{\mu}_h \;\middle|\; \boldsymbol{\mu}_h = \sum_{i=1}^N \boldsymbol{\mu}_i \delta(\mathbf{x} - \boldsymbol{\xi}_i),\ \boldsymbol{\mu}_i \in \mathbb{R}^3,\ \forall i = 1, \ldots, N\right\} \tag{12}$$

where $\delta(\cdot)$ is the Dirac measure at $\mathbf{x} = \mathbf{0}$. Then we shall use $\langle \cdot, \cdot \rangle_{B_h(t)}$ defined by

$$\langle \boldsymbol{\mu}_h, \mathbf{v}_h \rangle_{B_h(t)} = \sum_{i=1}^N \boldsymbol{\mu}_i \cdot \mathbf{v}_h(\boldsymbol{\xi}_i), \quad \forall \boldsymbol{\mu}_h \in \Lambda_h(t),\ \mathbf{v}_h \in W_{0,h} \tag{13}$$

Then we approximate $\Lambda_0(t)$ by

$$\Lambda_{0,h}(t) = \left\{\boldsymbol{\mu} \mid \boldsymbol{\mu} \in \Lambda_h(t),\ \langle \boldsymbol{\mu}, \mathbf{e}_i \rangle_{B_h(t)} = 0,\ \langle \boldsymbol{\mu}, \mathbf{e}_i \times \overrightarrow{\mathbf{Gx}} \rangle_{B_h(t)} = 0,\ i = 1, 2, 3\right\} \tag{14}$$

A typical choice of points for defining (12) is to take the grid points of the velocity mesh internal to the particle B and whose distance to the boundary of B is greater than, e.g. $h/2$, and to complete with selected points from the boundary of $B(t)$ (see, e.g., Fig. 2, for an example of selected points on the surface of $B(t)$). As we did for $\Lambda_h(t)$ and $\langle \cdot, \cdot \rangle_{B_h(t)}$, we define the finite dimensional space $\Lambda_{T,h}$ and the inner product $\langle \cdot, \cdot \rangle_{T_h}$ via a set of points of the velocity mesh internal to the region $\Omega \setminus \overline{\mathbf{T}}$ and whose distance to the surface of $\mathbf{T}$ is greater than, e.g. h, and a set of the points chosen from the surface of the cylinder $\mathbf{T}$.

Remark 5. In order to facilitate the construction of the finite dimensional space $\Lambda_{T,h}$ we slightly increased the size of the cross section of Ω, replacing thus this last cylinder by Ω_h. With this approach it is easier to select the collocation points used to force the condition $\mathbf{u} = \mathbf{0}$ outside $\mathbf{T}$ (see Section 4 for more details).

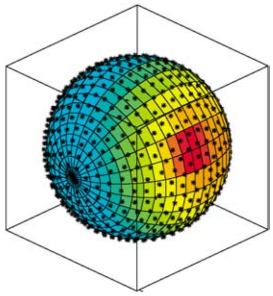

Fig. 2. An example of selected points on the boundary of the particle.

Remark 6. The inner product like bracket $\langle\cdot,\cdot\rangle_{B_h(t)}$ in (13) makes little sense for the continuous problem, but it is meaningful for the discrete problem; it amounts to forcing the rigid body motion of $B(t)$ via a *collocation method*. A similar technique has been used to enforce Dirichlet boundary conditions by Bertrand et al. [17].

Using the above finite dimensional spaces leads to the following approximation of problem (1)–(7) (where, for notational simplicity, we still denote by Ω the domain Ω_h introduced in Remark 5):

For a.e. $t>0$, find $\mathbf{u}_h(t)\in W_{0,h}$, $p(t)\in L^2_{0,h}$, $\mathbf{V}_\mathbf{G}(t)\in\mathbb{R}^3$, $\mathbf{G}(t)\in\mathbb{R}^3$

$\boldsymbol{\omega}(t)\in\mathbb{R}^3$, $\boldsymbol{\lambda}_h(t)\in\Lambda_{0,h}(t)$, $\boldsymbol{\lambda}_{T_h}\in\Lambda_{T,h}$ such that

$$\begin{cases} \rho_f\displaystyle\int_\Omega\left[\frac{\partial\mathbf{u}_h}{\partial t}+(\mathbf{u}_h\cdot\nabla)\mathbf{u}_h\right]\cdot\mathbf{v}\,\mathrm{d}\mathbf{x}+\mu_f\int_\Omega\nabla\mathbf{u}_h:\nabla\mathbf{v}\,\mathrm{d}\mathbf{x}\\ \quad-\displaystyle\int_\Omega p_h\nabla\cdot\mathbf{v}\,\mathrm{d}\mathbf{x}-\langle\boldsymbol{\lambda}_h,\mathbf{v}\rangle_{B_h(t)}-\langle\boldsymbol{\lambda}_{T_h},\mathbf{v}\rangle_{T_h}=\int_\Omega\mathbf{F}\cdot\mathbf{v}\,\mathrm{d}\mathbf{x},\quad\forall\mathbf{v}\in W_{0,h}\end{cases}\tag{15}$$

$$\int_\Omega q\nabla\cdot\mathbf{u}_h(t)\,\mathrm{d}\mathbf{x}=0,\quad\forall q\in L^2_h\tag{16}$$

$$\big\langle\boldsymbol{\mu},\mathbf{u}_h(t)\big\rangle_{B_h(t)}=0,\quad\forall\boldsymbol{\mu}\in\Lambda_{0,h}(t)\tag{17}$$

$$\big\langle\boldsymbol{\mu}_T,\mathbf{u}_h(t)\big\rangle_{T_h}=0,\quad\forall\boldsymbol{\mu}_T\in\Lambda_{T,h}\tag{18}$$

$$\frac{\mathrm{d}\mathbf{G}}{\mathrm{d}t}=\mathbf{V}_\mathbf{G}\tag{19}$$

$$\mathbf{V}_\mathbf{G}(0)=\mathbf{V}^0_\mathbf{G},\quad\boldsymbol{\omega}(0)=\boldsymbol{\omega}^0,\quad\mathbf{G}(0)=\mathbf{G}^0=\left\{G^0_1,G^0_2,G^0_3\right\}^t\tag{20}$$

$$\mathbf{u}_h(\mathbf{x},0)=\bar{\mathbf{u}}_{0,h}(\mathbf{x})\quad(\text{with }\nabla\cdot\bar{\mathbf{u}}_{0,h}=0)\tag{21}$$

Applying a first order operator splitting scheme à la Marchuk–Yanenko [18] (also see [11–13]) to discretize equations (15)–(21) in time, we obtain (after dropping some of the subscripts h):

$$\mathbf{u}^0=\bar{\mathbf{u}}_{0,h},\ \mathbf{V}^0_\mathbf{G},\ \boldsymbol{\omega}^0,\ \text{and }\mathbf{G}^0\text{ are given;}\tag{22}$$

for $n\geqslant 0$, knowing $\mathbf{u}^n$, $\mathbf{V}^n_\mathbf{G}$, $\boldsymbol{\omega}^n$ and $\mathbf{G}^n$, compute $\mathbf{u}^{n+\frac{1}{6}}$ and $p^{n+\frac{1}{6}}$ via the solution of

$$\begin{cases}\rho_f\displaystyle\int_\Omega\frac{\mathbf{u}^{n+\frac{1}{6}}-\mathbf{u}^n}{\Delta t}\cdot\mathbf{v}\,\mathrm{d}\mathbf{x}-\int_\Omega p^{n+\frac{1}{6}}\nabla\cdot\mathbf{v}\,\mathrm{d}\mathbf{x}=0,\quad\forall\mathbf{v}\in W_{0,h}\\ \displaystyle\int_\Omega q\nabla\cdot\mathbf{u}^{n+\frac{1}{6}}\,\mathrm{d}\mathbf{x}=0,\quad\forall q\in L^2_h;\ \mathbf{u}^{n+\frac{1}{6}}\in W_{0,h},\ p^{n+\frac{1}{6}}\in L^2_{0,h}\end{cases}\tag{23}$$

Then compute $\mathbf{u}^{n+\frac{2}{6}}$ via the solution of

$$\begin{cases} \int_\Omega \frac{\partial \mathbf{u}}{\partial t} \cdot \mathbf{v}\,\mathrm{d}\mathbf{x} + \int_\Omega \left(\mathbf{u}^{n+\frac{1}{6}} \cdot \nabla\right)\mathbf{u} \cdot \mathbf{v}\,\mathrm{d}\mathbf{x} = 0, \quad \forall \mathbf{v} \in W_{0,h}, \text{ a.e. on } \left(t^n, t^{n+1}\right) \\ \mathbf{u}\left(t^n\right) = \mathbf{u}^{n+\frac{1}{6}}; \quad \mathbf{u}(t) \in W_{0,h} \end{cases} \tag{24}$$

$$\mathbf{u}^{n+\frac{2}{6}} = \mathbf{u}\left(t^{n+1}\right) \tag{25}$$

Next, compute $\mathbf{u}^{n+\frac{3}{6}}$ and $\boldsymbol{\lambda}_{T_h}^{n+\frac{3}{6}}$ via the solution of

$$\begin{cases} \rho_f \int_\Omega \frac{\mathbf{u}^{n+\frac{3}{6}} - \mathbf{u}^{n+\frac{2}{6}}}{\Delta t} \cdot \mathbf{v}\,\mathrm{d}\mathbf{x} + \alpha\mu_f \int_\Omega \nabla\mathbf{u}^{n+\frac{3}{6}} \cdot \nabla\mathbf{v}\,\mathrm{d}\mathbf{x} \\ \quad - \left\langle \boldsymbol{\lambda}_{T_h}^{n+\frac{3}{6}}, \mathbf{v}\right\rangle_{T_h} = \int_\Omega \mathbf{F}^{n+1} \cdot \mathbf{v}\,\mathrm{d}\mathbf{x}, \quad \forall \mathbf{v} \in W_{0,h} \\ \left\langle \boldsymbol{\mu}_T, \mathbf{u}^{n+\frac{3}{6}}\right\rangle_{T_h} = 0, \quad \forall \boldsymbol{\mu}_T \in \Lambda_{T,h}; \;\; \mathbf{u}^{n+\frac{3}{6}} \in W_{0,h}, \boldsymbol{\lambda}_{T_h}^{n+\frac{3}{6}} \in \Lambda_{T,h} \end{cases} \tag{26}$$

Now predict the position and the translation velocity of the center of mass of the particle as follows:

Take $\mathbf{V}_\mathbf{G}^{n+\frac{4}{6},0} = \mathbf{V}_\mathbf{G}^n$ and $\mathbf{G}^{n+\frac{4}{6},0} = \mathbf{G}^n$; then predict the new position of the particle via the following sub-cycling and predicting–correcting technique:

For $k = 1, \ldots, N$, compute

$$\widehat{\mathbf{V}}_\mathbf{G}^{n+\frac{4}{6},k} = \mathbf{V}_\mathbf{G}^{n+\frac{4}{6},k-1} + \mathbf{F}^r\left(\mathbf{G}^{n+\frac{4}{6},k-1}\right)\Delta t/2N \tag{27}$$

$$\widehat{\mathbf{G}}^{n+\frac{4}{6},k} = \mathbf{G}^{n+\frac{4}{6},k-1} + \left(\widehat{\mathbf{V}}_\mathbf{G}^{n+\frac{4}{6},k} + \mathbf{V}_\mathbf{G}^{n+\frac{4}{6},k-1}\right)\Delta t/4N \tag{28}$$

$$\mathbf{V}_\mathbf{G}^{n+\frac{4}{6},k} = \mathbf{V}_\mathbf{G}^{n+\frac{4}{6},k-1} + \left(\mathbf{F}^r\left(\widehat{\mathbf{G}}^{n+\frac{4}{6},k}\right) + \mathbf{F}^r\left(\mathbf{G}^{n+\frac{4}{6},k-1}\right)\right)\Delta t/4N \tag{29}$$

$$\mathbf{G}^{n+\frac{4}{6},k} = \mathbf{G}^{n+\frac{4}{6},k-1} + \left(\mathbf{V}_\mathbf{G}^{n+\frac{4}{6},k} + \mathbf{V}_\mathbf{G}^{n+\frac{4}{6},k-1}\right)\Delta t/4N \tag{30}$$

enddo;

and let $\mathbf{V}_\mathbf{G}^{n+\frac{4}{6}} = \mathbf{V}_\mathbf{G}^{n+\frac{4}{6},N}$, $\mathbf{G}^{n+\frac{4}{6}} = \mathbf{G}^{n+\frac{4}{6},N}$. Compute $\mathbf{u}^{n+\frac{5}{6}}$ and $\boldsymbol{\lambda}^{n+\frac{5}{6}}$ via the solution of

$$\begin{cases} \rho_f \int_\Omega \frac{\mathbf{u}^{n+\frac{5}{6}} - \mathbf{u}^{n+\frac{3}{6}}}{\Delta t} \cdot \mathbf{v}\,\mathrm{d}\mathbf{x} + \beta\mu_f \int_\Omega \nabla\mathbf{u}^{n+\frac{5}{6}} \cdot \nabla\mathbf{v}\,\mathrm{d}\mathbf{x} = \left\langle \boldsymbol{\lambda}^{n+\frac{5}{6}}, \mathbf{v}\right\rangle_{B_h^{n+\frac{4}{6}}}, \quad \forall \mathbf{v} \in W_{0,h} \\ \left\langle \boldsymbol{\mu}, \mathbf{u}^{n+\frac{5}{6}}\right\rangle_{B_h^{n+\frac{4}{6}}} = 0, \quad \forall \boldsymbol{\mu} \in \Lambda_{0,h}^{n+\frac{4}{6}}; \;\; \mathbf{u}^{n+\frac{5}{6}} \in W_{0,h}, \;\; \boldsymbol{\lambda}^{n+\frac{5}{6}} \in \Lambda_{0,h}^{n+\frac{4}{6}} \end{cases} \tag{31}$$

and then solve for $\mathbf{V}_\mathbf{G}^{n+\frac{5}{6}}$ and $\boldsymbol{\omega}^{n+\frac{5}{6}}$ from $\mathbf{u}^{n+\frac{5}{6}}$

$$\begin{cases} \left\langle \mathbf{e}_i, \mathbf{u}^{n+\frac{5}{6}} - \mathbf{V}_\mathbf{G}^{n+\frac{5}{6}} - \boldsymbol{\omega}^{n+\frac{5}{6}} \times \overrightarrow{\mathbf{G}^{n+\frac{4}{6}}\mathbf{x}}\right\rangle_{B_h^{n+\frac{4}{6}}} = 0, & \text{for } i = 1, 2, 3 \\ \left\langle \mathbf{e}_i \times \overrightarrow{\mathbf{G}^{n+\frac{4}{6}}\mathbf{x}}, \mathbf{u}^{n+\frac{5}{6}} - \mathbf{V}_\mathbf{G}^{n+\frac{5}{6}} - \boldsymbol{\omega}^{n+\frac{5}{6}} \times \overrightarrow{\mathbf{G}^{n+\frac{4}{6}}\mathbf{x}}\right\rangle_{B_h^{n+\frac{4}{6}}} = 0, & \text{for } i = 1, 2, 3 \end{cases} \tag{32}$$

Finally, take $\mathbf{V}_\mathbf{G}^{n+1,0} = \mathbf{V}_\mathbf{G}^{n+\frac{5}{6}}$ and $\mathbf{G}^{n+1,0} = \mathbf{G}^{n+\frac{4}{6}}$; then predict the final position and translation velocity as follows:

For $k = 1, \ldots, N$, compute

$$\widehat{\mathbf{V}}_\mathbf{G}^{n+1,k} = \mathbf{V}_\mathbf{G}^{n+1,k-1} + \mathbf{F}^r\left(\mathbf{G}^{n+1,k-1}\right)\Delta t/2N \tag{33}$$

$$\widehat{\mathbf{G}}^{n+1,k} = \mathbf{G}^{n+1,k-1} + \left(\widehat{\mathbf{V}}_\mathbf{G}^{n+1,k} + \mathbf{V}_\mathbf{G}^{n+1,k-1}\right)\Delta t/4N \tag{34}$$

$$\mathbf{V}_\mathbf{G}^{n+1,k} = \mathbf{V}_\mathbf{G}^{n+1,k-1} + \left(\mathbf{F}^r\left(\widehat{\mathbf{G}}^{n+1,k}\right) + \mathbf{F}^r\left(\mathbf{G}^{n+1,k-1}\right)\right)\Delta t/4N \tag{35}$$

$$\mathbf{G}^{n+1,k} = \mathbf{G}^{n+1,k-1} + \left(\mathbf{V}_{\mathbf{G}}^{n+1,k} + \mathbf{V}_{\mathbf{G}}^{n+1,k-1}\right)\Delta t/4N \tag{36}$$

enddo;

and let $\mathbf{V}_{\mathbf{G}}^{n+1} = \mathbf{V}_{\mathbf{G}}^{n+1,N}$, $\mathbf{G}^{n+1} = \mathbf{G}^{n+1,N}$; and set $\mathbf{u}^{n+1} = \mathbf{u}^{n+\frac{5}{6}}$, $\boldsymbol{\omega}^{n+1} = \boldsymbol{\omega}^{n+\frac{5}{6}}$.

In the above algorithm (22)–(36), we have $t^{n+s} = (n+s)\Delta t$, $\Lambda_{0,h}^{n+s} = \Lambda_{0,h}(t^{n+s})$, B_h^{n+s} is the region occupied by the particle centered at $\mathbf{G}^{n+s}$, and $\mathbf{F}^r$ is a short range repulsion force which prevents the particle/particle and particle/wall penetration (see, e.g., [12,13]). Finally, α and β verify $\alpha + \beta = 1$; we have chosen $\alpha = 1$ and $\beta = 0$ for the numerical simulations to be discussed in Section 4.

3.1. Solutions of the subproblems (23), (24), (26) and (31)

To solve the *'degenerated' quasi-Stokes problem* (23), we employed a *preconditioned conjugate gradient* method introduced in [19] (see also [11] (Chapter 7)). In the above algorithm the preconditioning is achieved via the solution at each iteration of a discrete Poisson problem; to solve this last problem we used a matrix-free fast solver from FISHPAK, a package due to Adams, Swarztrauber and Sweet (see [20] for details). To solve the *pure advection problem* (24), we employed the *wave-like equation method* discussed in, e.g., [21], [11] (Chapter 6) and [22]. Unlike the two-dimensional flow investigated in [14], we have to solve here the two *saddle-point problems* (26) and (31). As in, e.g., [14], we used *conjugate gradient algorithms* to solve the two above problems. Actually, problems (26) and (31) are particular cases of

$$\begin{cases} \alpha \displaystyle\int_\Omega \mathbf{u}\cdot\mathbf{v}\,d\mathbf{x} + \mu \int_\Omega \nabla\mathbf{u} : \nabla\mathbf{v}\,d\mathbf{x} = \int_\Omega \mathbf{f}\cdot\mathbf{v}\,d\mathbf{x} + \langle\boldsymbol{\lambda}, \mathbf{v}\rangle, \quad \forall\mathbf{v}\in W_{0,h} \\ \langle\boldsymbol{\mu}, \mathbf{u}\rangle = 0, \quad \forall\boldsymbol{\mu}\in\Lambda;\ \mathbf{u}\in W_{0,h},\ \boldsymbol{\lambda}\in\Lambda \end{cases} \tag{37}$$

The conjugate gradient method for the solution of problem (37) reads as follows:

$$\boldsymbol{\lambda}^0 \in \Lambda \text{ is given} \tag{38}$$

solve

$$\begin{cases} \alpha \displaystyle\int_\Omega \mathbf{u}^0\cdot\mathbf{v}\,d\mathbf{x} + \mu \int_\Omega \nabla\mathbf{u}^0 : \nabla\mathbf{v}\,d\mathbf{x} = \int_\Omega \mathbf{f}\cdot\mathbf{v}\,d\mathbf{x} + \left\langle\boldsymbol{\lambda}^0, \mathbf{v}\right\rangle \\ \forall\mathbf{v}\in W_{0,h};\ \mathbf{u}^0\in W_{0,h} \end{cases} \tag{39}$$

then solve

$$\left\langle\mathbf{g}^0, \boldsymbol{\mu}\right\rangle = \left\langle\boldsymbol{\mu}, \mathbf{u}^0\right\rangle, \quad \forall\boldsymbol{\mu}\in\Lambda;\ \mathbf{g}^0\in\Lambda \tag{40}$$

and set

$$\mathbf{w}^0 = \mathbf{g}^0 \tag{41}$$

For $m \geqslant 0$, assuming that $\boldsymbol{\lambda}^m, \mathbf{u}^m, \mathbf{w}^m, \mathbf{g}^m$ are known, compute $\boldsymbol{\lambda}^{m+1}, \mathbf{u}^{m+1}, \mathbf{w}^{m+1}, \mathbf{g}^{m+1}$ as follows:
Solve

$$\begin{cases} \alpha \displaystyle\int_\Omega \bar{\mathbf{u}}^m\cdot\mathbf{v}\,d\mathbf{x} + \mu \int_\Omega \nabla\bar{\mathbf{u}}^m : \nabla\mathbf{v}\,d\mathbf{x} = \left\langle\mathbf{w}^m, \mathbf{v}\right\rangle \\ \forall\mathbf{v}\in W_{0,h};\ \bar{\mathbf{u}}^m\in W_{0,h} \end{cases} \tag{42}$$

and set

$$\left\langle\bar{\mathbf{g}}^m, \boldsymbol{\mu}\right\rangle = \left\langle\boldsymbol{\mu}, \bar{\mathbf{u}}^m\right\rangle, \quad \forall\boldsymbol{\mu}\in\Lambda;\ \bar{\mathbf{g}}^m\in\Lambda \tag{43}$$

Then compute

$$\rho_m = \left\langle\mathbf{g}^m, \mathbf{g}^m\right\rangle / \left\langle\bar{\mathbf{g}}^m, \mathbf{w}^m\right\rangle \tag{44}$$

and set

$$\boldsymbol{\lambda}^{m+1} = \boldsymbol{\lambda}^m - \rho_m\mathbf{w}^m, \quad \mathbf{u}^{m+1} = \mathbf{u}^m - \rho_m\bar{\mathbf{u}}^m, \quad \mathbf{g}^{m+1} = \mathbf{g}^m - \rho_m\bar{\mathbf{g}}^m \tag{45}$$

If $\langle \mathbf{g}^{m+1}, \mathbf{g}^{m+1}\rangle / \langle \mathbf{g}^0, \mathbf{g}^0\rangle \leqslant \epsilon$, then take $\mathbf{u} = \mathbf{u}^{m+1}$. If not, compute

$$\gamma_m = \langle \mathbf{g}^{m+1}, \mathbf{g}^{m+1}\rangle / \langle \mathbf{g}^m, \mathbf{g}^m\rangle \tag{46}$$

and set

$$\mathbf{w}^{m+1} = \mathbf{g}^{m+1} + \gamma_m \mathbf{w}^m \tag{47}$$

Do $m = m + 1$ and go back to (42).

Remark 7. When solving the saddle point problem (31), the finite dimensional multiplier space $\Lambda_{0,h}^{n+s}$ has to verify some constraints. Actually, the solution of the discrete variational problems (40) and (43) is achieved as follows:

(i) We observe first that both problems are particular cases of

$$\langle \mathbf{g}, \boldsymbol{\mu}\rangle_{B_h^{n+s}} = \langle \boldsymbol{\mu}, \mathbf{u}\rangle_{B_h^{n+s}}, \quad \forall \boldsymbol{\mu} \in \Lambda_{0,h}^{n+s};\ \mathbf{g} \in \Lambda_{0,h}^{n+s} \tag{48}$$

(ii) Next, we solve the *unconstrained problem*

$$\langle \tilde{\mathbf{g}}, \boldsymbol{\mu}\rangle_{B_h^{n+s}} = \langle \boldsymbol{\mu}, \mathbf{u}\rangle_{B_h^{n+s}}, \quad \forall \boldsymbol{\mu} \in \Lambda_{h}^{n+s};\ \tilde{\mathbf{g}} \in \Lambda_{h}^{n+s} \tag{49}$$

(iii) Then to obtain $\mathbf{g}$, project $\tilde{\mathbf{g}}$ into $\Lambda_{0,h}^{n+s}$ by finding $\mathbf{b} = \{b_1, b_2, b_3\}^t$ and $\mathbf{c} = \{c_1, c_2, c_3\}^t$ so that $\mathbf{b}$, $\mathbf{c}$ and $\mathbf{g}$ verify

$$\mathbf{g} = \tilde{\mathbf{g}} - \mathbf{c} - \mathbf{b} \times \overrightarrow{\mathbf{G}\mathbf{x}} \tag{50}$$

and

$$\begin{cases} \langle \mathbf{g}, \mathbf{e}_i\rangle_{B_h^{n+s}} = 0, & \text{for } i = 1, 2, 3 \\ \langle \mathbf{g}, \mathbf{e}_i \times \overline{\mathbf{G}^{n+s}\mathbf{x}}\rangle_{B_h^{n+s}} = 0, & \text{for } i = 1, 2, 3 \end{cases} \tag{51}$$

The resulting 6×6 linear systems are solved directly.

The procedure described in (i)–(iii) can be easily modified in order to handle the particle constrained motions mentioned in Remark 3. For these cases, when solving (32) to obtain $\mathbf{V}_{\mathbf{G}}^{n+\frac{5}{6}}$ and $\boldsymbol{\omega}^{n+\frac{5}{6}}$, one encounters a linear system similar to the above one.

4. Numerical experiments and discussion

4.1. One ball cases

For the first series of test problems, we consider the simulation of the constrained motion of a neutrally buoyant ball moving in a fluid filled cylinder. The ball center stays on a line parallel to Ox_3, and located below the cylinder axis in a vertical plane containing this axis; we suppose also that this ball is only allowed to rotate freely with respect to the x_1-axis as discussed in Remark 3. For (cross-)validation purposes, we will compare our results with those reported in [15], obtained by an arbitrary Lagrange–Euler technique involving a moving mesh. Following Remark 5, we take for computational domain is $\Omega = (0, 5 + 4h_v) \times (0, 5 + 4h_v) \times (0, 10)$, with h_v the space discretization step we use to construct the flow velocity spaces. The radius R of the cylinder is 2.5 and its length is 10. The radius of the ball is 0.375, while the common value of the densities of the fluid and ball is 1. The viscosity of the fluid is 1. The force $\mathbf{F}$ in (1) is a constant vector, positively oriented in the Ox_3 direction; $\|\mathbf{F}\|$ has been chosen so that the maximum velocity U_m of the corresponding *Poiseuille flow* (without particle) is 20 or 40. At $t = 0$, the ball mass center $\mathbf{G}(0)$ is vertically below the cylinder axis parallel to Ox_3, at a distance d_i from this axis which varies from $R/10$ to $3R/4$. We suppose that the ball is at rest initially and that the initial fluid velocity corresponds to the one of a fully developed Poiseuille flow whose maximal velocity U_m is either 20 or 40. We have used uniform tetrahedral meshes to approximate velocity and pressure. The velocity (resp., pressure) mesh size is $h_v = 1/20$ (resp., $h_p = 2h_v$), while the time discretization step is $\Delta t = 0.001$. Each case in Table 1 has been run during two time units and the reported values have been obtained by averaging the corresponding computed values on the time-interval [1.8, 2]. The results reported in Table 1 correspond to $U_m = 20$ and $U_m = 40$; they are in very good agreement with those reported in [15].

Table 1
Parameters for each computation (in columns 1, 2 and 7, 8) and comparisons (in columns 3–6 and 9–12) between the results computed by the methods in this article and those in [15]; V_{x_3} is the translation velocity in the Ox_3 direction and ω_{x_1} is the angular velocity with respect to the x_1 axis. The results with the superscript * are from [15]

U_m	d_i/R	V_{x_3}	$V^*_{x_3}$	ω_{x_1}	$\omega^*_{x_1}$	U_m	d_i/R	V_{x_3}	$V^*_{x_3}$	ω_{x_1}	$\omega^*_{x_1}$
20	0.10	19.4965	19.493	0.77513	0.78747	40	0.10	38.9781	38.398	1.5193	1.4897
20	0.20	18.8841	18.881	1.5514	1.5725	40	0.20	37.7295	37.424	3.0324	3.0309
20	0.30	17.8656	17.862	2.3235	2.3539	40	0.30	35.6716	35.618	4.5136	4.6092
20	0.40	16.4442	16.439	3.0872	3.1284	40	0.40	32.8297	32.833	5.9456	6.1050
20	0.50	14.6210	14.616	3.8409	3.8918	40	0.50	29.1910	29.159	7.3532	7.5560
20	0.60	12.3957	12.388	4.5824	4.6424	40	0.60	24.7773	24.763	8.7919	9.0370
20	0.70	9.73378	9.7052	5.2798	5.3295	40	0.70	19.5744	19.534	10.235	10.490
20	0.75	8.18216	8.1272	5.5765	5.5710	40	0.75	16.5464	16.472	10.873	11.028

Table 2
Parameters for each computation (in columns 1–2) and comparisons (in columns 3–8) between the results computed by the methods in this article and those in [15]; V_{x_3} and ω_{x_1} are as in the caption of Table 1 and d is the distance between the particle center of mass and the axis of the cylinder **T** parallel to Ox_3. The results with the superscript * are from [15]

U_m	d_i/R	d (d/R)	d^* (d^*/R)	V_{x_3}	$V^*_{x_3}$	ω_{x_1}	$\omega^*_{x_1}$
20	0.2	1.51448 (0.605792)	1.5027 (0.6108)	12.2353	12.364	4.635872	4.6513
20	0.75	1.51454 (0.605816)	1.5027 (0.6108)	12.2365	12.364	4.628561	4.6513
40	0.25	1.60718 (0.642872)	1.6041 (0.64164)	22.6388	22.558	9.474327	9.6591
40	0.75	1.60644 (0.642576)	1.6041 (0.64164)	22.6496	22.558	9.484843	9.6591

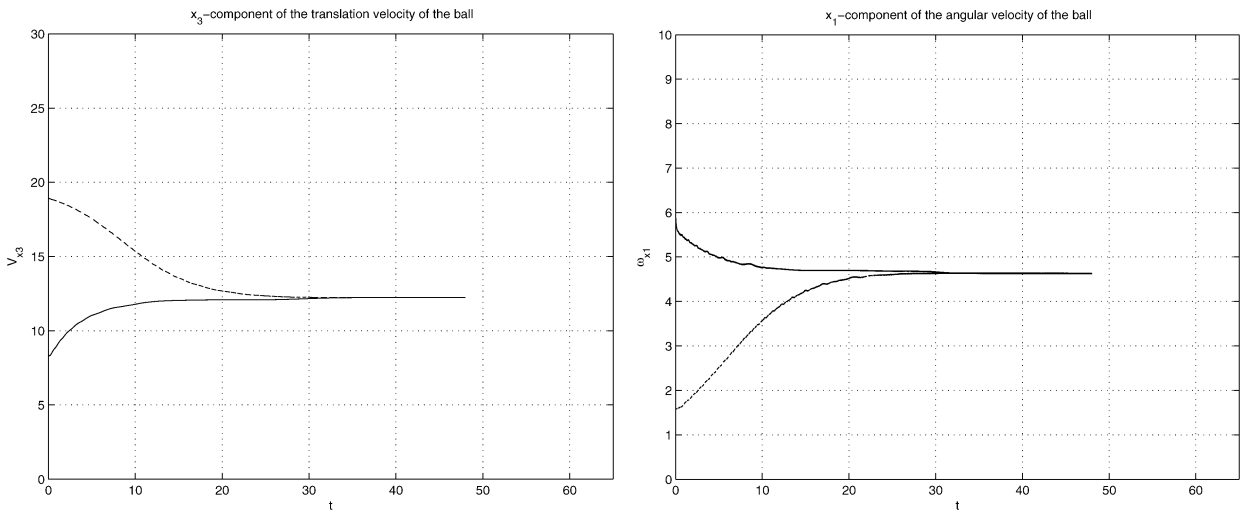

Fig. 3. Histories of the x_3 component of the translation velocity (left) and of the x_1 component of the angular velocity (right) when the maximal velocity U_m is 20. The dashed line (resp., solid line) corresponds to the case $d_i/R = 0.2$ (resp., the case $d_i/R = 0.75$).

For the cases where the ball is moving freely, we have chosen same set of parameters and initial conditions as in the above series of test problems, with one notable exception: namely, the initial distance d_i from the mass center of the ball to the central axis has been limited to those given in Table 2. In Table 2 we have shown the computed values of V_{x_3} and ω_{x_1} obtained once the ball reaches an *equilibrium position* and compare them with those reported in [15]. We observe the very good agreement between 'our' results and those in [15]; we observe also that the equilibrium distance is essentially independent of the ratio d_i/R. Assuming that the *characteristic length* is the diameter of the particle, the *particle Reynolds number* at the equilibrium is 9.18 (resp., 16.98) if $U_m = 20$ (resp., $U_m = 40$). In Figs. 3–5 we have shown the histories of (i) V_{x_3}, (ii) ω_{x_1}, and (iii) of the ratio d/R, where d is the distance between the ball center of mass and the cylinder axis parallel to Ox_3. As found in Karnis et al. [3], at the higher flow rate the particle moves closer to the wall of the cylinder and that the equilibrium position of the particle is reached faster, as shown in Fig. 5.

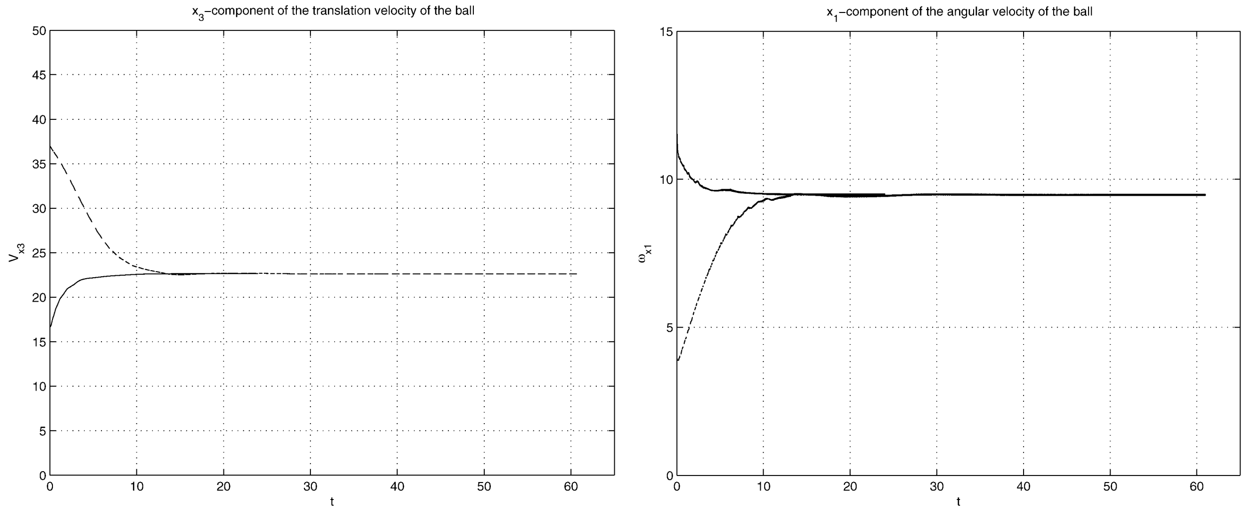

Fig. 4. Histories of the x_3 component of the translation velocity (left) and of the x_1 component of the angular velocity (right) when the maximal velocity U_m is 40. The dashed line (resp., solid line) corresponds to the case $d_i/R = 0.25$ (resp., the case $d_i/R = 0.75$).

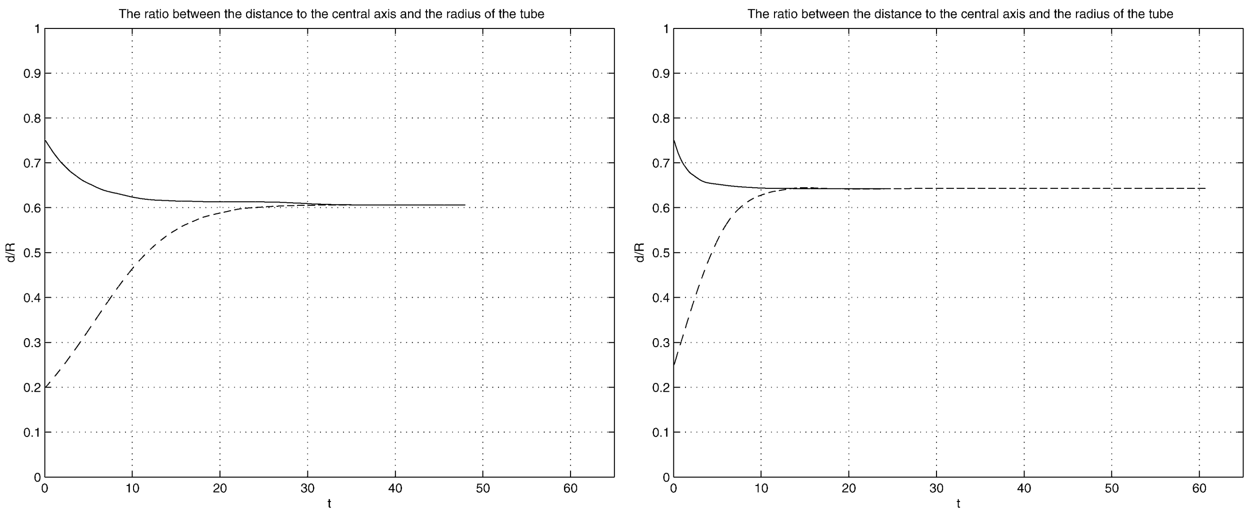

Fig. 5. Histories of the ratio of d/R for $U_m = 20$ (left) and $U_m = 40$ (right) for the freely moving neutrally buoyant ball.

For the velocity (resp., pressure) mesh size is $h_v = 1/20$ (resp., $h_p = 2h_v$), the number of velocity (resp., pressure) nodes is about 2.16×10^6 (resp., 270,440). The typical memory size for one test case is of the order of 320 Megabytes and it takes about 112 sec./time step on a 1.6 GHz AMD Athlon CPU.

Remark 8. Increasing L ($L = 10$ here) will not significantly modify the distance to the cylinder axis that the ball reaches as $t \to +\infty$ (for this range of particle Reynolds numbers, at least). As shown in previous calculations, our methodology can simulate particulate flow at larger particulate Reynolds numbers, but it will require a larger L and smaller h_v and h_p. Incidentally, for the case of one freely moving ball with $U_m = 20$, the tube Reynolds number is 61.2 taking the tube diameter as characteristic distance and the ball translation speed as characteristic velocity.

4.2. Five ball case

For this test case, we have considered the simulation of five neutrally buoyant balls moving ‘freely’ in a tube Poiseuille flow. Most parameters and initial conditions are as in the one ball situations discussed in Section 4.1, the

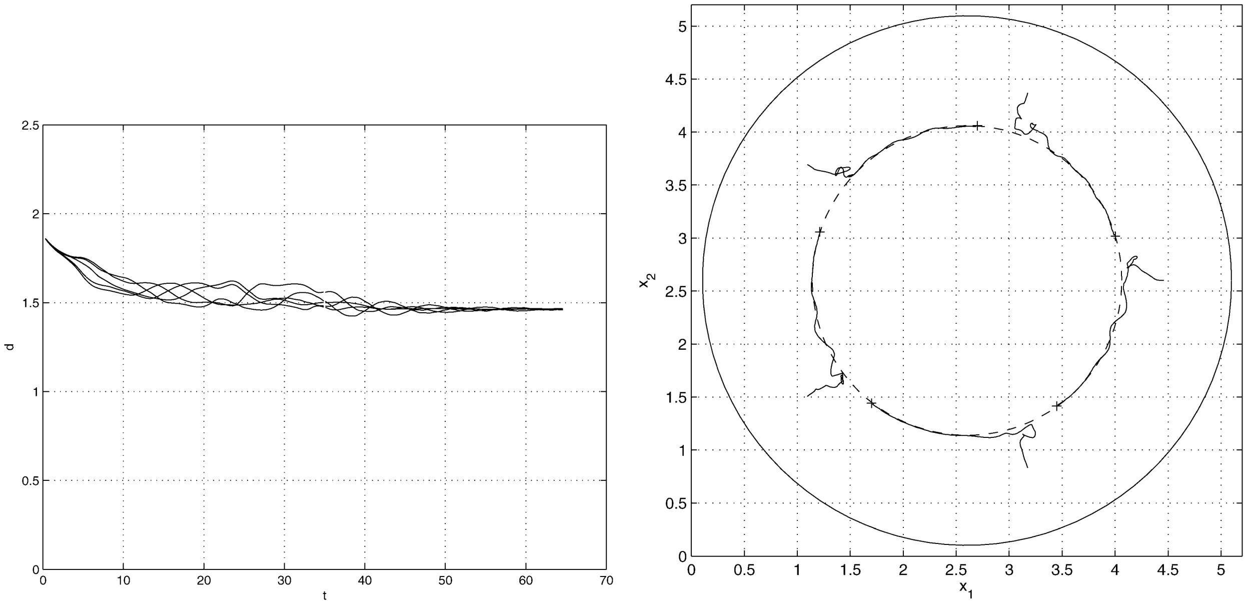

Fig. 6. Histories of the distances from the mass centers of the five balls to the central axis (left) and trajectories of the five balls viewed in the direction of the Ox_3-axis (right). In the right picture, the symbol '+' indicates the end of each ball center trajectory.

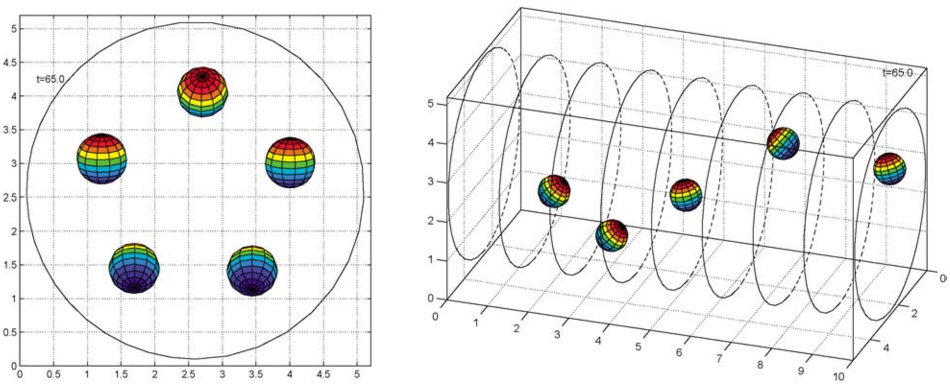

Fig. 7. Relative position of the five balls in the tube at $t = 65$.

only differences being: (i) U_m whose value is 20, here; and (ii) the initial position of the balls, which at $t = 0$ have their centers of mass located at the vertices of a regular pentagon contained in a plan orthogonal to Ox_3; the five particle have all their centers of mass located at the distance $0.75R$ from the axis of $\mathbf{T}$ parallel to Ox_3. As shown in Figs. 6 and 7, the five balls move closer to the cylinder axis and stabilize at a distance to the axis of the cylinder of the order of 0.585. On the other hand the initial co-planar configuration is lost, as shown in Fig. 7. Actually, we observe that the balls do not collide and, that, once they have reached their 'equilibrium' distance to the center of the cylinder, they rotate at an uniform velocity, the center of mass of each particle describing thus a kind of helicoid in the tube $\mathbf{T}$. The average velocity is of the order of 12.6 for $60 \leqslant t \leqslant 65$, implying thus that the averaged particle Reynolds number is about 9.45 (taking again the particle diameter as characteristic length). The side and front views of the five ball positions at $t = 65$ are shown in Fig. 7.

5. Conclusion

In [14] we developed a distributed Lagrange multiplier based fictitious domain method for simulating the motion of neutrally buoyant particles in pressure driven two-dimensional channel flow. In this article, we have generalized the above methodology so that it can handle three-dimensional variants of the particulate flow considered in [14]. For those test problems involving only one neutrally buoyant particle moving in a fluid filled cylinder, the numerical results are in very good agreement with the results reported in [15], which were obtained using an Arbitrary Euler–Lagrange method with moving mesh. In a near future, we will apply this methodology to cases involving particles with a more complicated shape, such as ellipsoids and cylinders.

Acknowledgements

We acknowledge the helpful comments and suggestions of E.J. Dean, J.W. He, H.H. Hu, P. Huang, D.D. Joseph, Y. Kuznetsov and G. Rodin. We thank also B.H. Yang and J. Wang for providing us with the details of their results reported in [15]. The support of NSF (grants ECS-9527123, CTS-9873236, DMS-9973318, CCR-9902035, and DMS-0209066) and DOE/LACSI (grant R71700K-292-000-99) is also acknowledged.

References

[1] G. Segré, A. Silberberg, Radial particle displacements in Poiseuille flow of suspensions, Nature 189 (1961) 209–210.
[2] G. Segré, A. Silberberg, Behavior of macroscopic rigid spheres in Poiseuille flow. Part I, J. Fluid Mech. 14 (1962) 115–157.
[3] A. Karnis, H.L. Goldsmith, S.G. Mason, The flow of suspensions through tubes. Part V: inertial effects, Canad. J. Chem. Engrg. 44 (1966) 181–193.
[4] H. Brenner, Hydrodynamic resistance of particles at small Reynolds numbers, Adv. Chem. Engrg. 6 (1966) 287–438.
[5] R.G. Cox, S.G. Mason, Suspended particles in fluid flow through tubes, Ann. Rev. Fluid Mech. 3 (1971) 291–316.
[6] L.G. Leal, Particle motions in viscous, Ann. Rev. Fluid Mech. 12 (1980) 435–476.
[7] F. Feuillebois, Some theoretical results for the motion of solid spherical particles in a viscous fluid, in: G.F. Hewitt, J.M. Delhaye, N. Zuber (Eds.), Multiphase Science and Technology, vol. 4, Hemisphere Pub. Corp., New York, 1989, pp. 583–798.
[8] J.B. McLaughlin, Inertial migration of a small sphere in linear shear flows, J. Fluid Mech. 224 (1991) 261–274.
[9] J. Feng, H.H. Hu, D.D. Joseph, Direct simulation of initial value problems for the motion of solid bodies in a Newtonian fluid. Part 2: Couette and Poiseuille flows, J. Fluid Mech. 277 (1994) 271–301.
[10] T. Inamuro, K. Maeba, F. Ogino, Flow between parallel walls containing the lines of neutrally buoyant circular cylinders, Int. J Multiphase Flow 26 (2000) 1981–2004.
[11] R. Glowinski, Finite element methods for incompressible viscous flow, in: P.G. Ciarlet, J.L. Lions (Eds.), Handbook of Numerical Analysis, vol. IX, North-Holland, Amsterdam, 2003, pp. 3–1176.
[12] R. Glowinski, T.-W. Pan, T. Hesla, D.D. Joseph, A distributed Lagrange multiplier/fictitious domain method for particulate flows, Int. J. Multiphase Flow 25 (1999) 755–794.
[13] R. Glowinski, T.-W. Pan, T. Hesla, D.D. Joseph, J. Périaux, A fictitious domain approach to the direct numerical simulation of incompressible viscous flow past moving rigid bodies: Application to particulate flow, J. Comput. Phys. 169 (2001) 363–426.
[14] T.-W. Pan, R. Glowinski, Direct simulation of the motion of neutrally buoyant circular cylinders in plane Poiseuille flow, J. Comput. Phys. 181 (2001) 260–279.
[15] B.H. Yang, J. Wang, D.D. Joseph, H.H. Hu, T.-W. Pan, R. Glowinski, Migration of a sphere in tube flow, J. Fluid Mech. 540 (2005) 109–131.
[16] M.O. Bristeau, R. Glowinski, J. Periaux, Numerical methods for the Navier–Stokes equations. Applications to the simulation of compressible and incompressible viscous flow, Comput. Phys. Rep. 6 (1987) 73–187.
[17] T. Bertrand, P.A. Tanguy, F. Thibault, A three-dimensional fictitious domain method for incompressible fluid flow problems, Int. J. Numer. Methods Fluids 25 (1997) 719–736.
[18] G.I. Marchuk, Splitting and alternating direction methods, in: P.G. Ciarlet, J.L. Lions (Eds.), Handbook of Numerical Analysis, vol. I, North-Holland, Amsterdam, 1990, pp. 197–462.
[19] R. Glowinski, T.-W. Pan, J. Périaux, Distributed Lagrange multiplier methods for incompressible flow around moving rigid bodies, Comput. Methods Appl. Mech. Engrg. 151 (1998) 181–194.
[20] J. Adams, P. Swarztrauber, R. Sweet, FISHPAK: A package of Fortran subprograms for the solution of separable elliptic partial differential equations, The National Center for Atmospheric Research, Boulder, CO, 1980.
[21] E.J. Dean, R. Glowinski, A wave equation approach to the numerical solution of the Navier–Stokes equations for incompressible viscous flow, C. R. Acad. Sci. Paris, Sér. I Math. 325 (1997) 783–791.
[22] T.-W. Pan, R. Glowinski, A projection/wave-like equation method for the numerical simulation of incompressible viscous fluid flow modeled by the Navier–Stokes equations, Comput. Fluid Dynamics J. 9 (2000) 28–42.